FTIR Study of ATP-Induced Changes in Na^+/K^+-ATPase from Duck Supraorbital Glands

Promod R. Pratap,* Oana Dediu,† and G. Ulrich Nienhaus†‡

*Department of Physics and Astronomy, University of North Carolina at Greensboro, Greensboro, North Carolina 27402-6710 USA; †Department of Biophysics, University of Ulm, 89069 Ulm, Germany; and ‡Department of Physics, University of Illinois at Urbana-Champaign, Urbana, Illinois 61801-3080 USA

ABSTRACT The Na^+/K^+-ATPase uses energy from the hydrolysis of ATP to pump Na^+ ions out of and K^+ ions into the cell. ATP-induced conformational changes in the protein have been examined in the Na^+/K^+-ATPase isolated from duck supraorbital salt glands using Fourier transform infrared spectroscopy. Both standard transmission and attenuated total internal reflection sample geometries have been employed. Under transmission conditions, enzyme at 75 mg/ml was incubated with dimethoxybenzoin-caged ATP. ATP was released by flashing with a UV laser pulse at 355 nm, which resulted in a large change in the amide I band. The absorbance at 1659 cm^{-1} decreased with a concomitant increase in the absorbance at 1620 cm^{-1}. These changes are consistent with a partial conversion of protein secondary structure from α-helix to β-sheet. The changes were ~8% of the total absorbance, much larger than those seen with other P-type ATPases. Using attenuated total internal reflection Fourier transform infrared spectroscopy, the decrease in absorbance at ~1650 cm^{-1} was titrated with ATP, and the titration midpoint $K_{0.5}$ was determined under different ionic conditions. In the presence of metal ions (Na^+, Na^+ and K^+, or Mg^{2+}), $K_{0.5}$ was on the order of a few μM. In the absence of these ions, $K_{0.5}$ was an order of magnitude lower (0.1 μM), indicating a higher apparent affinity. This effect suggests that the equilibrium for the ATP-induced conformational changes is dependent on the presence of metal ions.

INTRODUCTION

Na^+/K^+-ATPase (EC 3.6.1.3) is an integral membrane protein that uses the free energy liberated by hydrolysis of ATP to pump Na^+ and K^+ ions across the cell membrane (Glynn, 1985; Glynn and Karlish, 1975). For every mole of ATP hydrolyzed, the pump moves three moles of Na^+ out and two moles of K^+ into the cell. According to the Albers-Post scheme (Glynn, 1985; Glynn and Karlish, 1975), the enzyme exists in two major conformations. In the E_1 conformation, the enzyme has a high affinity for Na^+ and ATP and low affinity for K^+, and its cation binding sites face the cytoplasmic side of the membrane. In the E_2 conformation, the enzyme exhibits low affinity for Na^+ and ATP and high affinity for K^+, and its cation binding sites face the extracellular side of the membrane.

An abbreviated Albers-Post scheme is shown in Fig. 1. Starting in the upper left of the scheme, the first and fourth steps represent interactions between the monovalent cation binding sites on ATPase and the intracellular side of the membrane. In addition to ATP binding to the E_1 conformation with high affinity, ATP also binds to $E_2(2K^+)$ with low affinity and accelerates the fourth step. The second and third steps represent interactions between the monovalent cation binding sites on ATPase and the extracellular side of the membrane.

Enzyme activity is generally measured in the presence of Mg^{2+} and buffer containing high Na^+ and low K^+ ion concentrations. ATPase activity is then initiated by the addition of ATP. An activity assay as a function of ATP concentration reveals two apparent affinities for ATP: a high affinity in the range of a few μM associated with ATP binding to the E_1 conformation, and a low affinity of ~0.5 mM associated with ATP binding to the $E_2(2K^+)$ conformation (Post et al., 1965). Since ATP hydrolysis is governed by the rate-limiting step ($E_2(2K^+) \rightarrow E_1$), this measurement reveals the dependence of the rate-limiting step on ATP. The high apparent affinity of a few μM is also associated with the ATP-dependence of Na^+ transport and enzyme phosphorylation (Fahn et al., 1968; for ATP dependence of activity for the enzyme used in this study, see Martin and Sachs, 1999).

Association of ATP with the enzyme has been measured directly using a rate-of-dialysis or a centrifugation technique (Nørby and Jensen, 1988, 1971), yielding a dissociation coefficient K_d for ATP of ~0.1 μM, which is an order of magnitude smaller than the apparent affinity from the ATPase activity assay. The only way to reconcile these two measurements within the framework of the Albers-Post model is to assume that there is an additional step between the two steps probed in these experiments with a small equilibrium coefficient, thus favoring the reactant side of the reaction.

Earlier work had indicated that the release of ADP (first step in Fig. 1), Na^+ transport to the extracellular face (second step), hydrolysis and K^+ binding and occlusion (third step) are all essentially irreversible under conditions under which activity is measured (Glynn, 1985). It may be reasonable to hypothesize, therefore, that the step with the small equilibrium constant may have to do with conformational changes that occur immediately after ATP binds to the

Submitted January 16, 2003, and accepted for publication July 3, 2003.

Address reprint requests to Promod R. Pratap, Dept. of Physics and Astronomy, University of North Carolina at Greensboro, PO Box 26170, Greensboro, NC 27402-6710. E-mail: pratapp@uncg.edu.

0006-3495/03/12/3707/11 $2.00

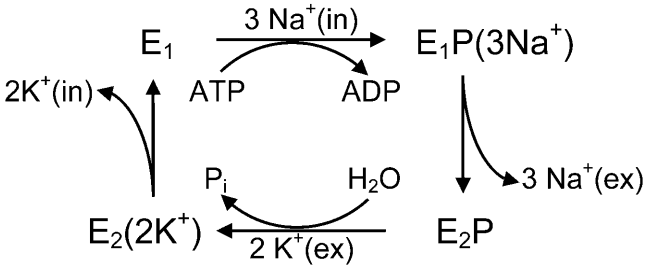

FIGURE 1 Albers-Post scheme for the reaction cycle of the Na^+, K^+-ATPase.

enzyme. Evidence of such conformational changes has been derived from infrared spectroscopy (Fringeli et al., 1989; Chetverin and Brazhnikov, 1985).

Recently, Toyoshima et al. (2000) used crystallographic techniques to determine the structure of the Ca^{2+}-ATPase from the sarcoplasmic reticulum (SERCA1) to a resolution of 2.6 Å. They concluded that ion transport and nucleotide binding results in large movements of subdomains within the protein. SERCA1 and the Na^+/K^+-ATPase belong to the same family of P-type ATPases and exhibit significant structural similarities (Sweadner and Donnet, 2001). The structure of the Na^+/K^+-ATPase at 11 Å resolution has been compared with that of SERCA1, and the gross structural features have been found to agree (Rice et al., 2001). Therefore, the SERCA1 structure may be used to interpret the infrared-spectroscopic observations presented here in terms of conformational changes.

Fourier transform infrared (FTIR) spectroscopy is a powerful tool that has been used widely to examine structural changes in proteins (see, for example, Vigano et al., 2000; Lamb et al., 2002; Braunstein et al., 1993; Mitchell et al., 1996; and references therein). It is an extremely sensitive technique that can monitor minute reaction-induced absorbance changes. Different strategies of sample preparation and reaction initiation have been developed. In transmission FTIR spectroscopy, a concentrated ATPase solution is sandwiched between two CaF_2 windows. The substrate ATP has been added to the sample in the form of a biologically inactive, UV-sensitive precursor compound. The ATPase reaction is then initiated by a short UV laser flash that rapidly converts this so-called ''caged ATP'' into the active form (von Germar et al., 2000; Scheirlinckx et al., 2001). An alternative approach, the attenuated total internal reflection (ATR) technique, allows in situ titration with substrate (Fringeli et al., 1989; Scheirlinckx et al., 2001; Vander Stricht et al., 2001). For ATR-FTIR spectroscopy, the sample is prepared on the surface of an IR-conducting crystal so that substrate can be exchanged with the buffer.

In IR studies of ATP-induced conformational changes in Na^+/K^+-ATPase and other P-type ATPases (von Germar et al., 2000; Barth et al., 1996; Barth and Mäntele, 1998; Scheirlinckx et al., 2001; Fringeli et al., 1989), ATP binding to the protein induced absorbance changes in the amide I and amide II regions of the IR spectrum, which were interpreted as a transition of the protein secondary structure from α-helical to a more β-sheet containing fold. Here, transmission-type and ATR-FTIR experiments have been used to study ATP-induced conformational changes in the E_1 conformation of Na^+/K^+-ATPase isolated from supraorbital salt glands of juvenile ducks. Unlike protein from other sources, this enzyme has near maximal enzymatic activity. We have observed absorbance changes with this enzyme that were by at least an order of magnitude larger than those previously reported. Hence it is particularly suited for infrared studies.

ATP-induced changes were examined as a function of ATP concentration in buffers containing Na^+, Na^+ and K^+, choline chloride, and choline chloride plus Mg^{2+}. All these ionic conditions are known to place the enzyme in the E_1 conformation (Glynn, 1985).

Experiments were intentionally *not* performed in the presence of K^+ alone because this condition would have prepared the enzyme in the $E_2(2K^+)$ conformation. As ATP binding is known to induce a transition from $E_2(2K^+) \rightarrow E_1$, the experiment would then monitor conformational changes associated with both ATP binding and the $E_2(2K^+) \rightarrow E_1$ conformational change, which would have complicated the interpretation of the results.

Preliminary data have already been presented at the 10th International Conference on Na,K-ATPase and Related Cation Pumps, August 8–14, 2002, in Elsinore, Denmark (Pratap et al., 2003).

MATERIALS AND METHODS

Enzyme preparation

All salts and buffers (reagent grade) were purchased from Sigma (St. Louis, MO) and Merck (Whitehouse Station, NJ). Na^+/K^+-ATPase microsomes were isolated from the supraorbital salt glands of young ducks, as described by Martin and Sachs (Martin and Sachs, 1999). Briefly, 12- to 14-day-old ducklings (Metzer Farms, Gonzales, CA) were grown for two weeks on standard poultry feed and ordinary tap water; in addition, the ducks were provided with several gallons of water for splashing. At the end of this period, the drinking water and the water in the splash pool (i.e., all water with which the ducks came in contact) was switched to 1% (w/v) saline in tap water. The ducks were euthanized with CO_2 after a further period of 10–12 days. The supraorbital salt glands were removed immediately and frozen in liquid nitrogen. The glands were minced, suspended in ice-cold homogenization buffer (20 mM Tris-HCl, pH 7.5, 1 mM EDTA, and 250 mM sucrose) at a concentration of 1 g of minced tissue per 10 ml of buffer and processed with a Polytron PT10/35 homogenizer (Kinematica, Cincinnati, OH). The homogenate was centrifuged for 15 min at 7,100 rpm in a Beckman clinical centrifuge (Model J2-21) with a JA20 rotor (Beckman Coulter USA, Fullerton, CA). The supernatant was saved. The pellet was resuspended in homogenization buffer and centrifuged as described above. The supernatants from the two spins were combined and centrifuged at 17,000 rpm for 1.5 h in a Beckman Ti50.2 rotor. The resulting pellet was resuspended in homogenization buffer and stored at −80°C. The protein concentration in the microsomal suspension was determined using a modified Lowry protein assay (Protein assay kit P5656, Sigma Diagnostics).

ATPase was purified from microsomes by partial extraction with SDS (Martin and Sachs, 1999). Microsomes (1 mg/ml) were incubated in buffer

(14 mM Tris-HCl, pH 7.5, 1.7 mM EDTA, 2.2 mM Na-ATP) at room temperature. A stock solution of SDS (2 mg/ml) was added slowly (over a period of 20 min) using a peristaltic pump (Mini variable pump, Fisher Scientific, Pittsburg, PA) to a final concentration of 0.55 mg/ml. The SDS-protein suspension was incubated at room temperature for 40 min. The suspension was then layered on a sucrose step gradient (w/v percent sucrose of 10:15:29.4:55) in Beckman Ultraclear tubes. The tubes were centrifuged at 25,000 rpm for 14–16 h. The band at the boundary between 29.4% and 55% was aspirated with a syringe. This solution was diluted with buffer (20 mM Tris-HCl, pH 7.5, 1 mM EDTA) and subsequently centrifuged at 50,000 rpm for 1 h using a Beckman Ti50.2 rotor. The pellet was resuspended in homogenization buffer and stored at −80°C. Protein was assayed using the modified Lowry assay as described above.

ATPase activity measurements

Enzyme activity was measured using a fluorescence-coupled enzyme assay (Banik and Roy, 1990; Pratap et al., 1997). Briefly, 10 ng of ATPase was added to a buffer containing 30 mM HEPES, pH 7.5, 1 mM EDTA, 130 mM NaCl, 20 mM KCl, 4 mM $MgCl_2$, 1 mM ATP, 25 μM 7-methylguanosine, and 0.15 units of bacterial purine nucleoside phosphorylase (PNP). PNP converts the fluorescent 7-methylguanosine to the nonfluorescent 7-methylguanine in the presence of inorganic phosphate (P_i) produced by ATP hydrolysis of the ATPase (Banik and Roy, 1990). The fluorescence change that accompanied this phosphorolytic reaction was followed in a fluorometer (Photon Technology International, South Brunswick, NJ; $\lambda_{ex} = 300$ nm, $\lambda_{em} = 410$ nm). The slope of the fluorescence change was proportional to the ATPase activity. All activity was measured at 37°C unless otherwise stated.

Transmission FTIR experiments

Transmission FTIR spectra were collected on an IFS-66v/S FTIR spectrometer (Bruker Optik, Ettlingen, Germany) at 2 cm^{-1} resolution. A frequency-tripled Nd-YAG laser (Surelite 10, Continuum, Santa Clara, CA) that emits 6-ns pulses at 355 nm was used to release ATP from its precursor DMB-caged ATP.

For the experiments, 12–15 μl enzyme suspension (5 mg/ml) in D_2O buffer (2 mM HEPES, pD 7.5, 0.1 mM EDTA, 2% (w/v) trehalose) and 0.2 μl of 9 mM DMB-caged ATP were mixed and dried under a gentle flow of N_2. The dried residue was resuspended in 0.8 μl of experiment buffer (20 mM HEPES, pD 7.5, 1 mM EDTA, 79 mM NaCl, and 20% (w/v) trehalose). This suspension was sandwiched between two circular CaF_2 windows separated by a Mylar ring of 8 μm thickness. The sandwich was mounted in a copper block and masked with copper tape, leaving a hole of 3 mm diameter for the IR beam to pass through the sample. The block was mounted onto a temperature-controlled holder and aligned inside the sample chamber, ensuring optimal alignment with respect to the IR beam and UV laser excitation. The chamber was continuously purged with dry air to minimize water vapor absorption.

After an initial transmission spectrum of the sample was taken, ATP was released by a UV pulse, and transmission spectra were taken as a function of time after the flash. Absorbance spectra were calculated with reference to the preflash spectrum. Absorbance bands were fitted with Gaussians, and the temporal development of the spectra was determined by analyzing the amplitude of the Gaussian as a function of time.

ATR-FTIR experiments

ATR-FTIR experiments were carried out using a Bruker ATR cell equipped with a germanium (Ge) crystal, which was 52.4 mm long, 10 mm wide, and 3.1 mm thick. In the crystal, the IR beam made eight reflections at an incident angle of 45° with respect to the surface. The crystal mount was modified extensively to allow for sealed operation and the possibility of solvent replacement. The ATR crystal in its holder was covered by a 2-mm thick Plexiglas sheet that was kept at a distance of 300 μm from the crystal surface by a silicone rubber gasket with a rectangular opening over the crystal that served as a sample chamber. At either end of the sample chamber formed by the gasket, a hole (0.8 mm diameter) was drilled into the Plexiglas cover which served as inlet and outlet of the sample chamber.

Before the experiments, the crystal was washed (in sequence) with 1), a 2% Helmanex solution in deionized water; 2), tap water; 3), deionized water; 4), ethanol; 5), methanol; and 6), hexane. Subsequently, the crystal was treated in a plasma cleaner. After mounting the crystal in the cell and assembling the Plexiglas cover, samples were introduced into the sample chamber using 1 ml tuberculin syringes (CODAN Medical ApS, Rødby, Denmark) with 0.8-mm needles that were cut a few mm from the Luer connector.

Sample preparation involved the formation of a palmitoyloleoylphosphatidylcholine (POPC) (Sigma) bilayer on top of the crystal with subsequent adhesion of membrane fragments to this bilayer (see below), using a modification of the protocol described by Fringeli et al. (1989). To observe the small, ATP-induced absorbance changes in the amide I region of the FTIR spectrum (~1650 cm^{-1}; Gerwert, 1999), where H_2O absorbs strongly, all aqueous solutions and buffers had to be prepared with D_2O.

Unilamellar POPC vesicles were obtained as follows: POPC (3.8 mg/ml) was dispersed in buffer with ionic strength equivalent to 100 mM Tris-HCl, pH 7.5, to form multilamellar vesicles. This suspension was freeze-thawed 10 times using liquid nitrogen and then passed 30 times through a polycarbonate membrane with a pore size of 50 nm using a LiposoFast extrusion apparatus (Avestin, Inc., Ottawa, Canada). The resulting vesicles were uniform, with a diameter of ~100 μm (MacDonald et al., 1991). The vesicle suspension was introduced into the sample chamber above the Ge crystal. Spontaneous formation of a bilayer could be observed by increases in the absorbance at 1465, 1731, 2852, and 2922 cm^{-1} and was complete in ~1 h. Excess POPC was then flushed out with buffer.

One day before the experiment, protein-containing membrane fragments were thawed and the equivalent of 1 mg protein was diluted with 2 ml of D_2O buffer. The suspension was spun down at 70,000 rpm for one hour at 4°C in a Beckman Optima TL tabletop ultracentrifuge using a TLA 100.2 rotor. The supernatant was discarded, and the pellet was resuspended in 1 ml of buffer. This suspension was stored overnight in a refrigerator. Before the experiments, the suspension was spun down again as described above. The supernatant was again discarded and the pellet resuspended in 0.2 ml of buffer (final concentration: 5 mg/ml protein).

After bilayer formation, membrane fragments (5 mg/ml protein) in the appropriate buffer were added to the sample chamber. Absorbance increases in the amide I region indicated fragment adhesion to the bilayer. This process was complete in 1 h after which excess membrane fragments were washed out with buffer. This preparation was stable for several hours. Varying amounts of ATP (vanadate-free Na salt from Sigma) were added to the sample chamber, and changes in absorbance were monitored.

Absorbance spectra were collected with one data point every 0.5 cm^{-1} and afterward averaged along the wavenumber axis over sets of 7 data points. A single Gaussian was then fitted to the data between 1630 and 1700 cm^{-1}. The amplitude of the Gaussian was plotted against ATP concentration to give a titration curve.

RESULTS

Transmission FTIR experiments

Transmission FTIR experiments were performed at 270 K (−3°C). Spectra of a Na^+/K^+-ATPase sample (94 mg/ml enzyme + 10.1 mM DMB-caged ATP) at 270 K were taken before and after flashing the sample with a 355 nm UV pulse. Fig. 2 shows a difference spectrum in the range 1100–2000 cm^{-1}, corrected with a linear baseline. Positive features refer

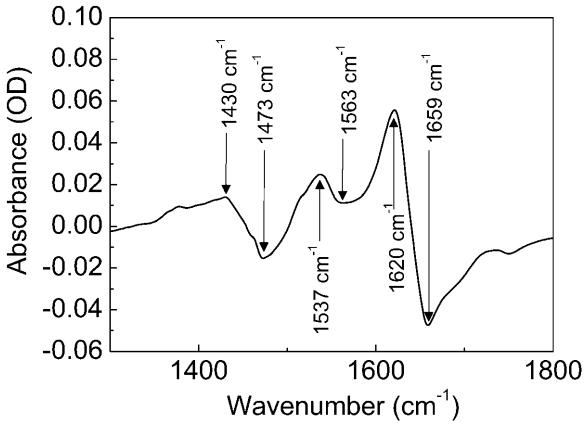

FIGURE 2 FTIR absorbance difference spectrum of enzyme (94 mg/ml) + DMB-caged ATP (10.1 mM) at 270 K, calculated from transmission spectra taken before and after the 355-nm uncaging pulse. Absorbance decreases at 1659 cm^{-1} (amide I), 1563 cm^{-1} and 1473 cm^{-1} (amide II of N–H and N–D, respectively) are indicative of a transition from α-helix to β-sheet.

to an absorbance increase due to the reaction, negative features to absorbance loss. Most pronounced are the changes in the amide I (backbone C=O stretch) region. The disappearance of absorbance at 1659 cm^{-1} with concomitant appearance of absorbance at 1620 cm^{-1} is usually assigned to a conversion from an α-helical structure to β-sheet upon ATP binding. The time dependence of this conformational change was monitored at 1659 cm^{-1} over 8000 s and fitted with two exponentials with time constants of $8.1 \pm 4.2 \times 10^2$ and $4.7 \pm 1.6 \times 10^3$ s (Fig. 3).

A secondary structure transition from α-helix to β-sheet is also supported by the changes seen in the amide II (N–H bend/C–N stretch) region (Fig. 2). We note a local minimum in the difference spectrum at 1563 cm^{-1} and a peak at 1536 cm^{-1} that can be explained by the secondary structure

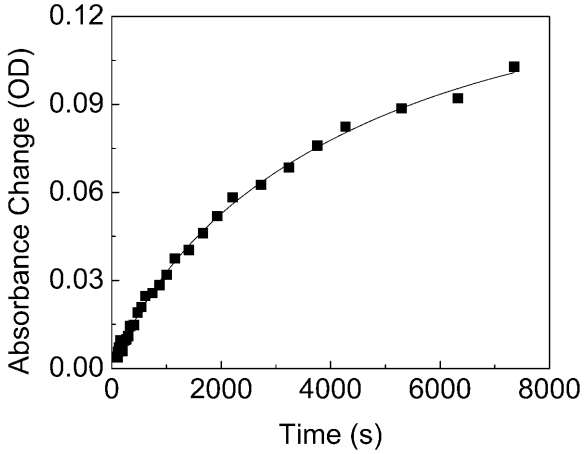

FIGURE 3 Time course of IR absorbance difference at 1659 cm^{-1}, induced by the release of ATP from DMB-caged ATP at 270 K in Na^+ buffer. The solid line is a fit with a sum of two exponentials with time constants of $8.1 \pm 4.2 \times 10^2$ and $4.7 \pm 1.6 \times 10^3$ s.

changes mentioned above. Because of partial exchange of the backbone hydrogen to deuterium, the negative feature at 1473 cm^{-1} is associated with the amide II (N–D bend/C–N stretch). Despite the sizable effects on the difference spectra, the number of residues involved in this conformational change may nevertheless be small. For a related P-type ATPase, an estimate of 3 to 10 amino acids involved in these structural changes was obtained (Barth et al., 1996).

Additional features occur in the difference spectrum in Fig. 2. In the region 1700–1800 cm^{-1}, where protonated carboxyl groups absorb without interference from other bands, a band at 1750 cm^{-1} disappears upon ATP binding. The bands in the region below 1300 cm^{-1} are assigned mainly to phosphate or P–O–P backbone vibrations.

The maximal absorbance difference of the sample shown in Fig. 3 was ~100 mOD at an estimated total sample absorbance at 1659 cm^{-1} of ~1 OD. Both absolute and relative changes upon ATP binding thus were at least an order of magnitude higher than the changes seen earlier with other P-type ATPases (von Germar et al., 2000; Scheirlinckx et al., 2001).

ATP release from DMB-caged ATP was examined by Sokolov et al. (1998). They estimated the ATP yield upon dissociation with a saturating flash of light as 7% of the initial concentration of caged ATP. We assume a similar value in this work. We have examined the time-course of ATP release at 270 K using a preparation of caged ATP without membrane fragments (data not shown). The dissociation process was already finished before the first scan was started. Thus, the absorbance changes in Figs. 2 and 3 are only associated with ATP binding and not influenced by photodissociation.

ATR-FTIR experiments: formation of bilayer

ATR-FTIR experiments were performed with membrane fragments adhered to a POPC bilayer formed spontaneously from POPC vesicles on a Ge crystal. Bilayer formation was followed in situ by observing absorbance changes in the methylene asymmetric and symmetric C–H stretch bands of the lipid at 2922 and 2852 cm^{-1}, respectively. Fig. 4 shows the absorbance of the vesicle suspension in the evanescent wave volume with respect to the absorbance of buffer. The kinetics of bilayer formation was examined by plotting the absorbance at 2922 cm^{-1} as a function of time (Fig. 5). The time dependence was analyzed by a fit with a biexponential function:

$$A(t) = A_0 + \Delta A_1\left[1 - \exp\left(-\frac{t}{\tau_1}\right)\right] + \Delta A_2\left[1 - \exp\left(-\frac{t}{\tau_2}\right)\right]. \quad (1)$$

For the data shown in Figs. 4 and 5, the two observed time constants were 22 ± 3 s and 590 ± 120 s. Consequently,

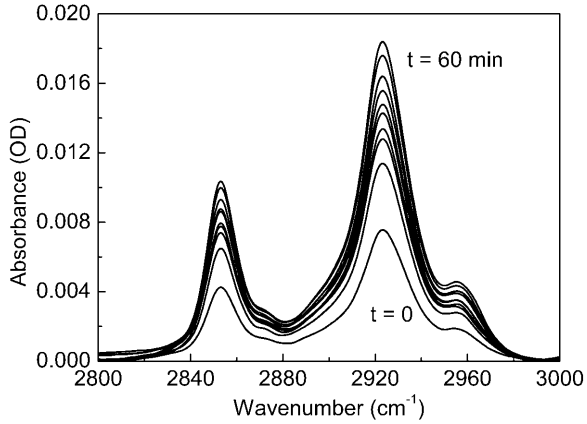

FIGURE 4 ATR-FTIR spectra in the C–H stretch region, monitoring spontaneous bilayer formation from POPC vesicles on the germanium ATR crystal as a function of time. Spectra were referenced to a buffer spectrum taken before the experiment.

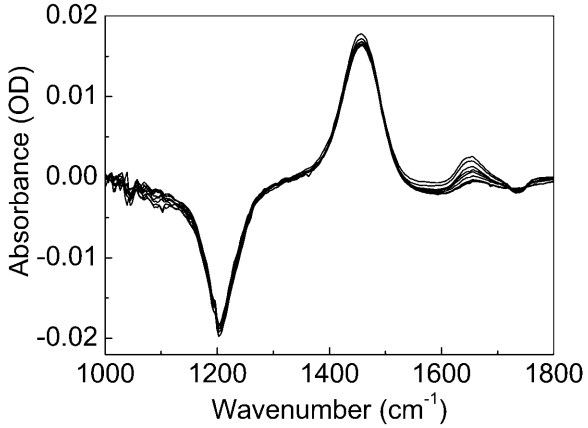

FIGURE 6 ATR-FTIR spectra of the temporal development of membrane fragment adhesion to the lipid bilayer. The spectra were referenced to a spectrum obtained after formation of the POPC bilayer in buffer and before membrane fragments (5 mg/ml) in buffer were added to the chamber.

bilayer formation is essentially complete within the first 10 minutes.

Adhesion of membrane fragments to the bilayer

After bilayer formation, the sample chamber was flushed with buffer, and a reference FTIR spectrum was taken. Subsequently, the chamber was perfused with a suspension of membrane fragments in buffer at a protein concentration of 5 mg/ml, and IR spectra were collected as a function of time over a period of an hour (Fig. 6). Most pronounced are two absorbance bands of opposite sign at 1202 and 1457 cm^{-1}. The negative band at 1202 cm^{-1} arises from the removal of D_2O from the volume probed by the evanescent wave, and the strong absorbance around 1457 cm^{-1}, which is assigned to the methylene bending vibration, signals the appearance of lipids. Adhesion of membrane fragments to the bilayer can also be observed by absorbance increases in the amide I and II regions (Fig. 6).

The amide I absorbance increase at 1645 cm^{-1} showed saturable and linear components. The total observed absorbance change (the sum of saturable and linear components) was ~3 mOD (Fig. 7 *A*). The data could be fitted to the following equation:

$$A(t) = A_0 + \Delta A_1 t + \Delta A_2\left[1 - \exp\left(-\frac{t}{\tau}\right)\right]. \qquad (2)$$

The fit, shown as a solid line in Fig. 7 *A*, yielded a time constant for fragment adhesion of 360 ± 130 s. This time constant is an order of magnitude larger than the faster

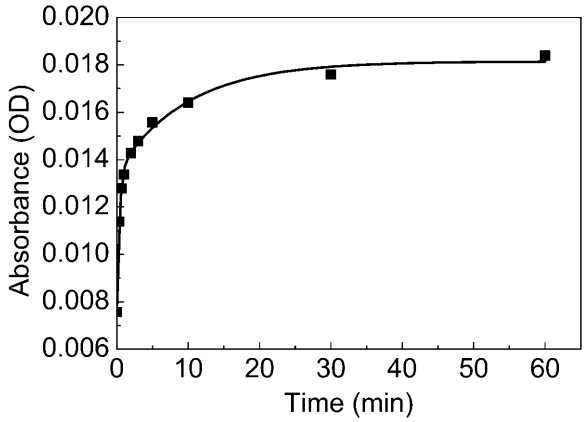

FIGURE 5 Kinetics of bilayer formation, as monitored as an increase in absorbance at 2922 cm^{-1} (Fig. 4). The solid curve is a fit with Eq. 1, with parameters $A_0 = 7.6 \pm 0.3 \times 10^{-3}$, $\Delta A_1 = 5.9 \pm 0.4 \times 10^{-3}$, $\tau_1 = 22 \pm 3$ s, $\Delta A_2 = 4.6 \pm 0.3 \times 10^{-3}$, and $\tau_2 = 590 \pm 120$ s.

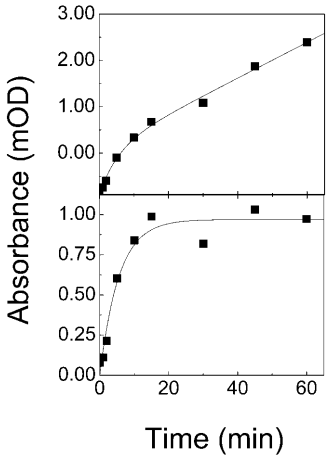

FIGURE 7 (*A*) Kinetics of membrane fragment adhesion, as observed from the absorbance change in the amide I band at 1645 cm^{-1}. The solid line is a fit with Eq. 2, yielding the parameters $A_0 = -0.89 \pm 0.08$ mOD, $\Delta A_1 = 6.5 \pm 0.5 \times 10^{-4}$ OD·s^{-1}, $\Delta A_2 = 1.0 \pm 0.2$ mOD, and time constant $\tau = 330 \pm 130$ s. (*B*) The data in (*A*) replotted after normalization and subtracting the linear contribution.

time constant for bilayer formation, and of the same order of magnitude as the slower time constant for bilayer formation. To show the saturable component more clearly, the data were replotted after subtracting the linear contribution $A_0 + \Delta A_1 \cdot t$ (Fig. 7 *B*).

The saturable component may represent membrane adhesion directly to the bilayer, whereas the linear component may represent the subsequent settling of membrane fragments on top of the bilayer plus membrane fragments, forming multiple layers of membrane fragments. The first process is saturable because the surface area of the bilayer available for fragment adhesion is limited. The second process, strictly speaking, will have complex kinetics. Even if the settling of the membrane fragments were to proceed at a constant rate, the evanescent volume decays exponentially with distance above the crystal, thus resulting in an exponential time-dependence of the second process. However, if the time constant of this exponential is large compared to the time of observation, only the linear portion in the series expansion of the exponential will be observed in the experiment described here.

It is possible to obtain a rough estimate for this time constant from the sedimentation velocity using the Svedberg equation (Berg, 1993). With 1.17 g/cm^3 as the density of the membrane fragments (estimated from the density of the sucrose solutions used in the preparation of these fragments) and an average fragment diameter of 0.2 μm, we calculate a settling velocity of 10^{-11} m/s. Assuming the thickness of the evanescent volume to be on the order of 1 μm, we obtain a value of 10^5 s, or ~1 day, which is much longer than the duration of the experiment.

In the experiments described here, membrane fragment adhesion was halted after 1 h by flushing the volume above the crystal with buffer. Since the absorbance due to the membrane fragments did not change after flushing, the settled membrane fragments were not removed by this procedure.

Titration of ATPase with ATP

Addition of ATP resulted in a saturable decrease in absorbance at ~1650 cm^{-1}. This decrease can be attributed to a transition from α-helix to β-sheet (von Germar et al., 2000). Fig. 8 shows some representative data from a typical ATP titration experiment. As seen from the difference spectrum in Fig. 2, this decrease in absorbance is accompanied by a concomitant increase at 1620 cm^{-1}. However, there is an additional contribution from ATP in solution at 1623 cm^{-1}, as observed when the sample chamber was perfused with ATP in the absence of bilayer and membrane fragments (results not shown).

Therefore, only the absorbance decrease at ~1650 cm^{-1} was taken as an indicator of ATP binding to the enzyme and quantified as a function of ATP concentration. Because the absorbance changes were small (typically several hundred μOD), Gaussians were fitted to the FTIR absorbance

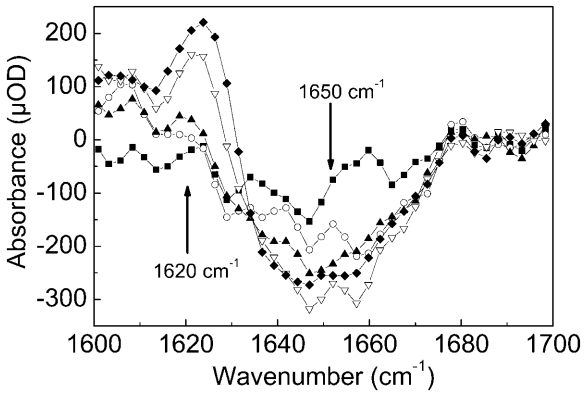

FIGURE 8 ATP-induced absorbance change in membrane fragments. After fragment adhesion, the chamber above the crystal was flushed with buffer and then filled with ATP-containing buffer at different concentrations. Curves for 500 nM (■), 5 μM (○), 50 μM (▲), 500 μM (▽) and 1 mM (◆) are shown here. These curves were generated as described in the Materials and Methods section. The absorbance change at ~1650 cm^{-1} was monitored as an indicator of ATP-induced conformational changes in the ATPase.

between 1630 and 1700 cm^{-1}. Comparison with the overall absorbance of the sample at that wavenumber (~3 mOD for the sample shown in Fig. 8) yields a relative absorbance change of ~10%. The amplitudes of the Gaussians as a function of ATP concentration were taken to obtain a titration curve (Fig. 9).

For each experimental condition, the titration data could be fitted by one rectangular hyperbola and a straight line:

$$A(t) = A_0 + \Delta A_1[ATP] + \Delta A_2 \frac{[ATP]}{K + [ATP]}. \qquad (3)$$

Here, [*ATP*] denotes the concentration of ATP. Because the slope of the linear term varied with experiments done under different conditions, the straight lines were subtracted

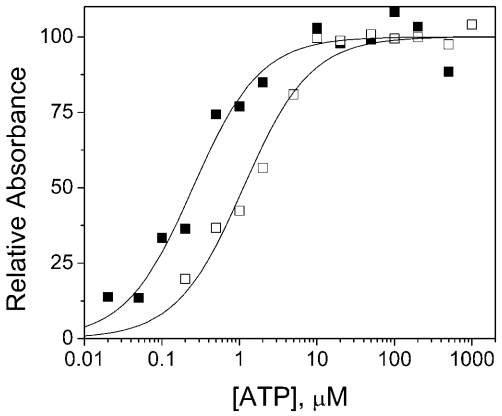

FIGURE 9 Absorbance at ~1650 cm^{-1} as a function of ATP concentration, for enzyme in choline buffer (■) and enzyme in Na^+ buffer (□). The solid lines are fits to rectangular hyperbolae. The $K_{0.5}$ for this experiment with choline buffer was 0.25 μM, and for the experiments with Na^+ buffer was 1.8 μM. Data for these and other experiments are summarized in Table 1.

from the data before comparison. The titration data, normalized to the saturation value of the absorbance change, are presented in Fig. 9 for experiments done using buffer containing choline chloride and buffer containing choline chloride + Mg^{2+}.

These experiments were repeated under various salt conditions: in buffer containing Na^+, Na^+ plus K^+, choline, or choline plus Mg^{2+}. In all cases, the total concentration of monovalent cations was maintained constant. The apparent affinities of the enzyme for ATP under these conditions are shown in Table 1. In the presence of Na^+, Na^+ plus K^+, or Mg^{2+}, the apparent affinity was on the order of a few μM. In the absence of these ions, i.e., in the presence of choline alone, the apparent affinity was $\sim$0.1 μM.

DISCUSSION

Transmission FTIR experiments

In earlier studies of nucleotide-induced conformational changes of the Na^+/K^+-ATPase and other P-type ATPases using transmission FTIR, the signals were relatively small (Chetverin et al., 1980; Scheirlinckx et al., 2001; von Germar et al., 2000). In the experiments presented here, the signals were at least an order of magnitude larger than those seen earlier. There are two possible reasons for this difference. 1), In this study, enzyme from the supraorbital salt glands of young ducks was used, which has been shown to exhibit near-maximal specific activity (Martin and Sachs, 1999). Enzyme from other sources is known to be only partially active (Fringeli et al., 1989; Chetverin and Brazhnikov, 1985). 2), Earlier work used caged ATPs that have been shown to bind to the enzyme already in the caged form (Forbush, 1984; Nagel et al., 1987; Borlinghaus and Apell, 1988; Sokolov et al., 1998). The aim of the present study was to monitor binding-induced structural changes in the enzyme. To avoid binding of caged ATP to the ATP binding sites with concomitant structural changes in the protein before ATP release, we used DMB-caged ATP in this study, which has been suggested not to bind to the ATPase (Sokolov et al., 1998). However, because the large relative size of the signal was observed both in the transmission FTIR and in the ATR-FTIR experiments, and caged ATP was not used in the ATR-FTIR experiments, we conclude that the source of enzyme is responsible for the large spectral changes.

TABLE 1 Half-maximal ATP concentrations for ATP-induced absorbance changes

Experimental conditions	$K_{0.5}$ (μM)	Number of experiments
Na buffer	3.1	2
Na/K buffer	2.1	2
Choline buffer, −Mg*	0.11	4
Choline buffer, +Mg	3.1	2

*In experiments with choline alone, [*ATP*] was varied from 10 nM to 1 mM. In all other experiments, [*ATP*] was varied from 200 nM to 1 mM. [*ATP*] denotes the concentration of ATP.

Bilayer formation

The kinetics of bilayer formation was followed by monitoring the absorbance in the methylene asymmetric stretch at 2922 cm^{-1} as a function of time. The absorbance (Fig. 5) was fitted with a sum of two exponentials (Eq. 1), yielding estimates of the five parameters in the equation. The initial absorbance A_0 was 7.6 $\pm$ 0.3 mOD; the changes in absorbance were $\Delta A_1 = 5.9 \pm 0.4$ and $\Delta A_2 = 4.6 \pm 0.3$, with the corresponding time constants $\tau_1 = 22 \pm 3$ s and $\tau_2 = 590 \pm 120$ s. Although there is some uncertainty regarding the precise zero point in this experiment, a major fraction of the first spectrum measured, and thus the initial absorbance, is expected to represent the absorbance of the POPC vesicle suspension. The thickness of the layer probed by the evanescent wave at 2922 cm^{-1} (defined as the average over the integral of the decay) may be estimated to be $\sim$0.5 μm (Harrick, 1967).

The POPC deposited on the surface per unit area may be estimated as follows. The absorbance increase (characterized by $\Delta A = \Delta A_1 + \Delta A_2$) may be attributed to the extra POPC that accumulates in the evanescent volume due to bilayer formation. The extent of bilayer formation can be estimated by comparing ΔA with A_0. First, the extent of the evanescent volume above 1 μm^2 of the crystal is 0.5 μm^3, or 5×10^{-16} l. The initial concentration of POPC was 5 mM, and this corresponded to an absorbance of 7.6 mOD. The formation of the bilayer resulted in an absorbance increase of $\Delta A =$ 10.5 mOD, or an apparent increase in concentration by 6.9 mM, all of which may be assumed to be in the bilayer. Therefore, the number of moles of POPC that is in the bilayer over 1 μm^2 of crystal was calculated to be 3.5×10^{-18} moles·μm^{-2}, or 2.1×10^{18} molecules per m^2. In these calculations, the extinction coefficient of POPC in suspension was assumed to be the same as that in the bilayer.

Note that both leaflets of the bilayer were made with POPC. The density of POPC in one of the leaflets would be 1.8×10^{-18} moles·μm^{-2}. Fringeli et al. (1989) deposited a monolayer of POPC on a Ge crystal previously coated with dipalmitoylphosphatidylcholine (DPPC). In that work, they estimated that the concentration of POPC deposited on the surface as a monolayer was 2.28×10^{-18} moles μm^{-2}. A direct comparison of these values indicates that the method used here to lay a bilayer on the Ge crystal covers 79% of the area covered by the bilayer in the experiments of Fringeli et al. (1989).

These values may be different due to several reasons. Fringeli et al. (1989) formed bilayers on the crystal using the Langmuir-Blodgett technique, which may cover a larger fraction of the Ge crystal than covered here: note that the method used here covers only the surface of the crystal

contained within the sample chamber, whereas the measurement probes the surface of the entire crystal. Further, Fringeli et al. (1989) measured the absorbance of the bilayer using polarized light. The difference in absorbance between polarized and unpolarized light at 2922 cm^{-1} may be estimated to be ~10% (Silvestro and Axelsen, 1998; Harrick, 1967).

The calculations presented above are based on the assumption that the constant A_0 represents the initial absorbance of lipid in suspension. Since there was a delay between the addition of lipid vesicles to the sample chamber and the initiation of measurement, it is likely that some lipid already adhered to the crystal during this time. This delay was not quantified, but it is possible to place an upper limit on it. Consider the extreme case where the absorbance of the lipid vesicles in suspension is negligible (almost zero). Then, the initial absorbance A_0 is due to the absorbance of lipid that adhered to the crystal before the start of measurement (the ''dead time'' of the experiment). This dead time can be estimated from Eq. 1 and the fitted parameters from Fig. 5 to be 18 s. Therefore, the dead time of the experiment could not have been greater than 18 s.

If the dead time of the experiments was ~10 s, then the initial absorbance A_0 would have been 4.2 mOD, and ΔA would have been 13.9 mOD. This indicates an apparent increase in POPC concentration of 16.5 mM. Following the same logic as earlier, the density of lipids deposited on the surface would be 4.3×10^{-18} moles/μm^2.

Membrane fragment adhesion

The results reported here indicate that the membrane fragments adhere to the bilayer at a slower rate than that of bilayer formation. Adhesion was monitored as an increase in absorbance at 1650 cm^{-1}. Because the change in absorbance is small, it was difficult to determine an adequate baseline for the data at this wavenumber. However, the change in absorbance was attributable to the membrane fragments adhered to the lipid bilayer. Since the ATP-induced absorbance changes were monitored at 1650 cm^{-1}, this absorbance was assumed to be the sample absorbance with respect to the lipid bilayer plus buffer.

ATP-induced absorbance changes

The volume above the membrane bilayer with adherent membrane fragments was perfused with buffer containing varying concentrations of ATP. Addition of ATP induced decreases in infrared absorbance at ~1650 cm^{-1}, attributable to conformational transitions from α-helix to β-sheet (von Germar et al., 2000). The maximal absorbance change for the data shown in Figs. 8 and 9 was ~250 μOD, which is 8% of the overall absorbance of ~3 mOD, consistent with the absorbance change that was observed upon addition of ATP under transmission conditions (Figs. 2 and 3).

It must be noted that with the present data, it is not possible to decide if the absorbance changes are due to large changes localized in the cytoplasmic loop between the M4 and M5 transmembrane domains or a sum of smaller changes that occurred throughout the protein (the $\alpha\beta$-protomer). It is possible that some of the observed signal originates in the β-subunit: Lutsenko and Kaplan (1994) have shown that ligand binding to the protein induces conformational changes in the β-subunit, and Farley and co-workers (Eakle et al., 1992, 1994, 1995) have demonstrated that changes in the β-subunit alters the properties of the protein.

It is possible, however, to estimate the number of amino acids involved in the changes. The number of amino acids in α-helical conformation can be estimated on the basis of the structural similarity between the α-subunit of the Na^+/K^+-ATPase and SERCA1 (Sweadner and Donnet, 2001; Rice et al., 2001). Moreover, the α-subunit of the duck ATPase is closely related to the chicken α_1-isoform (D. W. Martin, personal communication). Although the structure of the duck β-subunit is not known, it is reasonable to assume that the β-subunit is also related to the β_1-isoform from chicken. The amino acid sequence of the chicken β-subunit has been published in the GenBank, along with its one putative transmembrane segment

From these structural similarities, one may deduce that 38% of SERCA1 and 9% of the β-subunit are α-helical. This implies that a total of 409 amino acids in the $\alpha\beta$-protomer are α-helical. Thus, our experimentally observed 8% change in α-helical structure translates into 33 amino acids in the whole protein that are involved in the helix-sheet transition. The structure of SERCA1 also indicates that 58 amino acids in the N-domain (involved in nucleotide binding) are α-helical. If the helix-sheet transition involves transitions in the N-domain alone, slightly more than half the amino acids in this region are involved in this transition.

The current data can also be compared with published data for Na^+/K^+-ATPase from the shark rectal gland. Heimburg et al. (1997) have estimated that ~35% of this enzyme is α-helical. From their data, ~55% of this α-helical structure are in the transmembrane portion of the protein. An 8% change in helix structure involves 28 amino acids. Considering the lack of crystallographic data for this enzyme, this result is consistent with the estimates presented here from SERCA1. A further assumption that the helix-sheet transition occurs in the extramembranous helices of the protein (45% of the helix structure) implies that ~15% of the extramembranous α-helical structure changes to β-sheet as a result of ATP binding.

Our results and conclusions do not agree with those of Barth et al. (1996), who found small ATP-induced changes in the Ca^{2+}-ATPase (3–10 amino acids). This discrepancy is probably due to the different caged-ATP used in that study: they used *P*3-1-(2-nitro)phenylethyladenosine 5′-triphosphate (NPE-caged ATP), which has been shown to bind to the ATPase already in the caged form (Sokolov et al., 1998;

Forbush, 1984; Borlinghaus and Apell, 1988). Therefore, a large fraction of the binding-associated conformational changes may have occurred before uncaging.

The apparent affinity (as represented by $K_{0.5}$) calculated from ATP-induced changes in IR absorbance was around a few μM. This is consistent with the $K_{0.5}$ for ATP in ATPase activity measurements and for the E_1P to E_2P conformational change (Glynn, 1985; Glynn and Karlish, 1975), but at least an order of magnitude higher than the K_d for ATP binding as measured by dialysis (Nørby and Jensen, 1988).

These results may be interpreted in terms of the following model:

$$E_1 + ATP \leftrightarrow E_1 - ATP \leftrightarrow E_1 \sim ATP \leftrightarrow \cdots\cdots \leftrightarrow E_2(2K^+) \leftrightarrow E_1 \qquad \text{Scheme 1}$$

This scheme is a modified version of the standard Albers-Post reaction scheme (Fig. 1). The second step in the scheme has been added to represent a conformational change in the protein subsequent to ATP binding. This is the step that is probed by the absorbance change at $\sim$1650 cm^{-1}; it will be referred to as the FTIR-sensitive step in this discussion. This step must necessarily occur before phosphorylation, because the current experiments were done under conditions that preclude phosphorylation (absence of either Na^+ or Mg^{2+}). In the complete Albers-Post scheme, several steps occur between the FTIR-sensitive step and the rate-limiting step of the reaction cycle (the last step in Scheme 1). These include enzyme phosphorylation, conformational change from E_1P and E_2P, enzyme dephosphorylation, and K^+ binding and occlusion within the enzyme.

The dependence of ATPase activity on ATP measured the kinetics of the last step in Fig. 1 and Scheme 1. Dialysis experiments (Nørby and Jensen, 1988) measured the kinetics of ATP association to the enzyme—i.e., the first step shown above. FTIR experiments reported here measured the kinetics of the second step in the scheme.

Dialysis experiments estimated an apparent K_d for ATP binding of $\sim$0.1 μM (Nørby and Jensen, 1988). On the other hand, estimates of an apparent K_d for ATPase activity was of the order of a few μM (Glynn, 1985; Glynn and Karlish, 1975). It is obvious, therefore, that there must be a step between ATP binding and the $E_2(K) \rightarrow E_1$ transition with a small equilibrium constant, favoring the reactant side of that reaction step.

The experimental results reported here indicate that the $K_{0.5}$ of ATP for the α-helix-to-β-sheet transition is similar to that for enzyme activity and higher than the K_d for ATP binding as measured by dialysis. Therefore, the identity of this step may be narrowed to the region in the reaction sequence which includes steps 1 and 2 in Scheme 1. Since the first step is the high-affinity binding of ATP, the second step must be the step with small equilibrium constant.

An argument as to why the conformational change itself may be the step with the small equilibrium coefficient is presented as follows. The magnitude of the FTIR signal corresponding to a transition from α-helix to β-sheet indicates that it involves fairly large rearrangements of the protein—an 8% change in absorbance must involve at least an 8% α-helix to β-sheet interconversion.

Titration experiments under varying ionic conditions

The ATR-FTIR experiments described here were performed in the presence of different ions: *a*), 79 mM NaCl; *b*), 74 mM NaCl + 5 mM KCl; *c*), 79 mM choline chloride; and *d*), 79 mM choline chloride + 4 mM $MgCl_2$. The apparent affinities under conditions *a*, *b*, and *d* were comparable, whereas the affinity under condition *c* was at least an order of magnitude higher. The absence of cations with specific binding sites on the protein (Na^+, K^+, and Mg^{2+}) appears to shift the ATP-induced conformational change probed by infrared spectroscopy to the right (i.e., increasing the equilibrium coefficient). The nature of this novel effect on the ATPase is unclear at this time. It is not consistent with the Hofmeister series for cations (Hasselbach and Migala, 1998).

Currently, we do not know in which way these ions affect the ATPase, but the results reported here are consistent with those of Mårdh and Post (1977), who found that the presence of Na^+ increased the dissociation constant of ATP from the E_1 conformation of the enzyme (by a factor of 2) as compared with the dissociation of ATP from the enzyme in the absence of metal ions. This result is consistent with the data reported here, comparing those in the absence of metal ions (Table 1, row 3) with those in the presence of Na^+ in the buffer (Table 1, row 1).

CONCLUSIONS

The infrared absorption spectrum of the Na^+/K^+-ATPase is sensitive to conformational changes induced by ATP binding to the protein. In this work, the kinetics of these changes has been examined using FTIR spectroscopy.

Under the conditions used here, the amide I infrared absorption, measured in transmission geometry, changed by $\sim$8%, which is at least an order of magnitude more than the changes observed with Na^+/K^+-ATPase (Chetverin et al., 1980) from other sources and with other P-type ATPases (Scheirlinckx et al., 2001; von Germar et al., 2000). Transient-state kinetics of ATP-induced conformational changes was examined using DMB-caged ATP at 270 K.

ATP-induced conformational changes were measured as a function of ATP concentration using ATR-FTIR spectroscopy. The titration midpoint $K_{0.5}$ for ATP was similar to that for ATPase activity, but at least an order of magnitude larger than that for ATP binding measured by dialysis techniques. These experiments support the existence of an early step in the reaction sequence of the ATPase with a low equilibrium

coefficient, in which the reverse reaction is strongly favored. The conformational change itself is a likely candidate for this step.

The authors thank Karin Nienhaus for help in the data analysis.

This work was supported by the National Science Foundation, Grant No. 0072563 to PRP, and the Deutsche Forschungsgemeinschaft (SFB 569-A4) to GUN.

REFERENCES

Banik, U., and S. Roy. 1990. A continuous fluorimetric assay for ATPase activity. *Biochem. J.* 266:611–614.

Barth, A., and W. Mäntele. 1998. ATP-induced phosphorylation of the sarcoplasmic reticulum Ca^{2+} ATPase: molecular interpretation of infrared difference spectra. *Biophys. J.* 75:538–544.

Barth, A., F. von Germar, W. Kreutz, and W. Mäntele. 1996. Time-resolved infrared spectroscopy of the Ca^{2+}-ATPase: the enzyme at work. *J. Biol. Chem.* 271:30637–30646.

Berg, H. C. 1993. Random Walks in Biology. Princeton University Press, Princeton, NJ.

Borlinghaus, R., and H. J. Apell. 1988. Current transients generated by the Na^+/K^+-ATPase after an ATP concentration jump: dependence on sodium and ATP concentration. *Biochim. Biophys. Acta.* 939:197–206.

Braunstein, D. P., K. Chu, K. D. Egeberg, H. Frauenfelder, J. R. Mourant, G. U. Nienhaus, P. Ormos, S. G. Sligar, B. A. Springer, and R. D. Young. 1993. Ligand binding to heme proteins: III. FTIR studies of His-E7 and Val-E11 mutants of carbonmonoxymyoglobin. *Biophys. J.* 65: 2447–2454.

Chetverin, A. B., and E. V. Brazhnikov. 1985. Do sodium and potassium forms of Na,K-ATPase differ in their secondary structure? *J. Biol. Chem.* 260:7817–7819.

Chetverin, A. B., S. Y. Venyaminov, V. I. Emelyanenko, and E. A. Burstein. 1980. Lack of gross protein structure changes in the working cycle of (Na^+,K^+)-dependent adenosinetriphosphatase. Evidence from infrared and intrinsic fluorescence spectroscopy data. *Eur. J. Biochem.* 108:149–156.

Eakle, K. A., M. A. Kabalin, S. G. Wang, and R. A. Farley. 1994. The influence of beta subunit structure on the stability of Na^+/K^+-ATPase complexes and interaction with K^+. *J. Biol. Chem.* 269:6550–6557.

Eakle, K. A., K. S. Kim, M. A. Kabalin, and R. A. Farley. 1992. High-affinity ouabain binding by yeast cells expressing Na^+,K^+-ATPase alpha subunits and the gastric H^+, K^+-ATPase beta subunit. *Proc. Natl. Acad. Sci. USA.* 89:2834–2838.

Eakle, K. A., R. M. Lyu, and R. A. Farley. 1995. The influence of beta subunit structure on the interaction of Na^+/K^+-ATPase complexes with Na^+. A chimeric beta subunit reduces the Na^+ dependence of phosphoenzyme formation from ATP. *J. Biol. Chem.* 270:134937–13947.

Fahn, S., G. J. Koval, and R. W. Albers. 1968. Sodium-potassium-activated adenosine triphosphatase of *Electrophorus* electric organ. V. Phosphorylation by adenosine triphosphate-^{32}P. *J. Biol. Chem.* 243:1993–2002.

Forbush, B. 1984. Na^+ movement in a single turnover of the Na pump. *Proc. Natl. Acad. Sci. USA.* 81:5310–5314.

Fringeli, U. P., H. J. Apell, M. Fringeli, and P. Läuger. 1989. Polarized infrared absorption of Na^+/K^+-ATPase studied by attenuated total reflection spectroscopy. *Biochim. Biophys. Acta.* 984:301–312.

Gerwert, K. 1999. Molecular reaction mechanisms of proteins monitored by time-resolved FTIR-spectroscopy. *Biol. Chem.* 380:931–935.

Glynn, I. M. 1985. The Na^+, K^+-transporting adenosine triphosphatase. *In* The Enzymes of Biological Membranes, 2nd ed. A. N. Martonosi, editor. Plenum Press, New York. 3:35–114.

Glynn, I. M., and S. J. D. Karlish. 1975. The sodium pump. *Annu. Rev. Physiol.* 35:13–55.

Harrick, N. J. 1967. Internal Reflection Spectroscopy. John Wiley and Sons, New York.

Hasselbach, W., and A. Migala. 1998. Cations and anions as modifiers of ryanodine binding to the skeletal muscle calcium release channel. *J. Membr. Biol.* 164:215–227.

Heimburg, T., M. Esmann, and D. Marsh. 1997. Characterization of the secondary structure and assembly of the transmembrane domains of trypsinized Na,K-ATPase by Fourier transform infrared spectroscopy. *J. Biol. Chem.* 272:25685–25692.

Lamb, D. C., K. Nienhaus, A. Arcovito, F. Draghi, A. E. Miele, M. Brunori, and G. U. Nienhaus. 2002. Structural dynamics of myoglobin: ligand migration among protein cavities studied by Fourier transform infrared/temperature derivative spectroscopy. *J. Biol. Chem.* 277: 11636–11644.

Lutsenko, S., and J. H. Kaplan. 1994. Molecular events in close proximity to the membrane associated with the binding of ligands to the Na,K-ATPase. *J. Biol. Chem.* 269:4555–4564.

MacDonald, R. C., R. I. MacDonald, B. P. Menco, K. Takeshita, N. K. Subbarao, and L. R. Hu. 1991. Small-volume extrusion apparatus for preparation of large, unilamellar vesicles. *Biochim. Biophys. Acta.* 1061:297–303.

Mårdh, S., and R. L. Post. 1977. Phosphorylation from adenosine triphosphate of sodium- and potassium-activated adenosine triphosphatase. Comparison of enzyme-ligand complexes as precursors to the phosphoenzyme. *J. Biol. Chem.* 252:633–638.

Martin, D. W., and J. R. Sachs. 1999. Preparation of Na^+,K^+-ATPase with near maximal specific activity and phosphorylation capacity: evidence that the reaction mechanism involves all of the sites. *Biochemistry.* 38:7485–7497.

Mitchell, D. M., J. D. Müller, R. B. Gennis, and G. U. Nienhaus. 1996. FTIR study of conformational substates in the CO adduct of cytochrome c oxidase from Rhodobacter sphaeroides. *Biochemistry.* 35:16782–16788.

Nagel, G., K. Fendler, E. Grell, and E. Bamberg. 1987. Na^+ currents generated by the purified (Na^+ and K^+)-ATPase on planar lipid membranes. *Biochim. Biophys. Acta.* 901:239–249.

Nørby, J. G., and J. Jensen. 1971. Binding of ATP to brain microsomal ATPase. Determination of the ATP-binding capacity and the dissociation constant of the enzyme-ATP complex as a function of K^+-concentration. *Biochim. Biophys. Acta.* 233:104–116.

Nørby, J. G., and J. Jensen. 1988. Measurement of binding of ATP and ADP to Na^+,K^+-ATPase. *Methods Enzymol.* 156:191–201.

Post, R. L., A. K. Sen, and A. S. Rosenthal. 1965. A phosphorylated intermediate in adenosine triphosphate-dependent sodium and potassium transport. *J. Biol. Chem.* 240:1437–1445.

Pratap, P. R., E. H. Hellen, A. Palit, and J. D. Robinson. 1997. Transient kinetics of substrate binding to Na^+/K^+-ATPase measured by fluorescence quenching. *Biophys. Chem.* 69:137–151.

Pratap, P. R., N. Olden-Stahl, O. Dediu, and G. U. Nienhaus. 2003. Interaction between ATP and the Na/K-ATPase from duck supraorbital salt glands. *Ann. N. Y. Acad. Sci.* 986:293–295.

Rice, W. J., H. S. Young, D. W. Martin, J. R. Sachs, and D. L. Stokes. 2001. Structure of Na^+,K^+-ATPase at 11 Å resolution: comparison with Ca^{2+}-ATPase in E_1 and E_2 states. *Biophys. J.* 80:2187–2197.

Scheirlinckx, F., R. Buchet, J. M. Ruysschaert, and E. Goormaghtigh. 2001. Monitoring of secondary and tertiary structure changes in the gastric H^+/K^+-ATPase by infrared spectroscopy. *Eur. J. Biochem.* 268:3644–3653.

Silvestro, L., and P. H. Axelsen. 1998. Infrared spectroscopy of supported lipid monolayer, bilayer, and multibilayer membranes. *Chem. Phys. Lipids.* 96:69–80.

Sokolov, V. S., H. J. Apell, J. E. Corrie, and D. R. Trentham. 1998. Fast transient currents in Na,K-ATPase induced by ATP concentration jumps from the P3-[1-(3′,5′-dimethoxyphenyl)-2-phenyl-2-oxo]ethyl ester of ATP. *Biophys. J.* 74:2285–2298.

Sweadner, K. J., and C. Donnet. 2001. Structural similarities of Na,K-ATPase and SERCA, the Ca2+-ATPase of the sarcoplasmic reticulum. *Biochem. J.* 356:685–704.

Toyoshima, C., M. Nakasako, H. Nomura, and H. Ogawa. 2000. Crystal structure of the calcium pump of sarcoplasmic reticulum at 2.6 Å resolution. *Nature*. 405:647–655.

Vander Stricht, D. V., V. Raussens, K. A. Oberg, J. M. Ruysschaert, and E. Goormaghtigh. 2001. Difference between the E_1 and E_2 conformations of gastric H^+/K^+-ATPase in a multilamellar lipid film system. Characterization by fluorescence and ATR-FTIR spectroscopy under a continuous buffer flow. *Eur. J. Biochem.* 268:2873–2880.

Vigano, C., L. Manciu, F. Buyse, E. Goormaghtigh, and J. M. Ruysschaert. 2000. Attenuated total reflection IR spectroscopy as a tool to investigate the structure, orientation and tertiary structure changes in peptides and membrane proteins. *Biopolymers*. 55:373–380.

von Germar, F., A. Barth, and W. Mäntele. 2000. Structural changes of the sarcoplasmic reticulum Ca^{2+}-ATPase upon nucleotide binding studied by Fourier transform infrared spectroscopy. *Biophys. J.* 78: 1531–1540.